A 60-year atmospheric nitrate isotope record from a Southeast Greenland ice core with minimal post-depositional alteration

Zhao Wei[1], Shohei Hattori[1,2,3*], Asuka Tsuruta[3], Zhuang Jiang[4], Sakiko Ishino[5], Koji Fujta[6], Sumito Matoba[7], Lei Geng[4], Alexis Lamothe[8], Ryu Uemura[6], Naohiro Yoshida[3,9,10], Joel Savarino[8], and Yoshinori Iizuka[7]

[1]International Center for Isotope Effects Research (ICIER), Nanjing University, Nanjing 210023, China

[2]Frontiers Science Center for Critical Earth Material Cycling, State Key Laboratory for Mineral Deposits Research, School of Earth Sciences and Engineering, Nanjing University, Nanjing 210023, China

[3]Department of Chemical Science and Engineering, School of Materials and Chemical Technology, Tokyo Institute of Technology, Kanagawa 226-8502, Japan

[4]School of Earth and Space Sciences, University of Science and Technology of China, Hefei, Anhui, China

[5]Institute of Nature and Environmental Technology, Kanazawa University, Kakuma-machi, Kanazawa, Ishikawa 920-1192, Japan

[6]Graduate School of Environmental Studies, Nagoya University, Nagoya, Japan

[7]Institute of Low-Temperature Science, Hokkaido University, Sapporo, Japan

[8]Univ. Grenoble Alpes, CNRS, IRD, INRAE, G-INP, Institut des Géosciences de l'Environnement, Grenoble, France

[9]National Institute of Information and Communications Technology, Koganei, Tokyo 184-8795, Japan

[10]Earth-Life Science Institute (ELSI), Institute of Science Tokyo, Tokyo 152-8550, Japan

Correspondence to: Shohei Hattori (hattori@nju.edu.cn)

Abstract. Stable isotopes of atmospheric nitrate (NO_3^-) are valuable tools for tracing nitrogen sources and processes; however, their signals in ice core records are often disrupted by post-depositional processes. The ice core from the southeastern Dome (SE-Dome) in Greenland is a potential record of variations in atmospheric chemistry that has experienced less post-depositional effects owing to a high accumulation rate (~1 m water equivalent per year). Herein, we report 60-year (1959–2014) $\delta^{15}N(NO_3^-)$ and $\Delta^{17}O(NO_3^-)$ records from the SE-Dome ice core. $\delta^{15}N(NO_3^-)$ decreased from 1960 to 1974 and exhibited clear seasonal changes (high in summer and low in winter). $\Delta^{17}O(NO_3^-)$ did not exhibit any significant long-term trends, but did contain seasonal patterns. The mass-weighted annual average of $\delta^{15}N(NO_3^-)$ values in the SE-Dome core were 4.2 ± 2.8 ‰ lower than those in the Greenland Summit ice core between 1959–2006. The Transfer of Atmospheric Nitrate Stable Isotopes To the Snow (TRANSITS) model under the SE-Dome condition estimated changes of only 0.9 ‰ in $\delta^{15}N(NO_3^-)$ and −0.2 ‰ in $\Delta^{17}O(NO_3^-)$ from the initial deposition. Although differences in the source of NO_3^- cannot be discounted, the lower $\delta^{15}N(NO_3^-)$ values observed at the SE-Dome compared to the Summit were likely due to reduced post-depositional alteration. Therefore, the SE-Dome ice core NO_3^- record offers a precise reconstruction of nitrogen oxides (NO_x) emissions from both North America and Western Europe, as well as atmospheric oxidation chemistry and transport, thereby providing reliable insight into atmospheric nitrogen cycling.

1 Introduction

Nitrate (NO_3^-) and its precursors (NO_x = NO + NO_2) play important roles in the atmosphere. Tropospheric NO_x cycling produces ozone (O_3), a key component of the atmospheric oxidative capacity (Finlayson et al., 1999). NO_x emitted from various sources, undergoes oxidation to form HNO_3, which contributes to acid rain (Shammas et al., 2020) and particulate matter (as NO_3^-, Zhai et al., 2021), and upon deposition, alters nutrient balance in ecosystems (Duce et al., 2008). Owing to increasing fossil fuel and chemical fertilizer use since the beginning of the Industrial Revolution, NO_x levels in the atmosphere have increased, which is reflected in the elevated NO_3^- concentrations in ice cores, including those collected from Greenland (Neftel et al., 1985; Mayewski et al., 1986). Despite efforts to curb NO_x emissions through pollution mitigation measures and NO_x removal including three-way catalytic converters, the decline in ice core NO_3^- concentrations has been relatively gradual, as observed in Greenland (Iizuka et al., 2017) and in an Alpine ice core (Eichler et al., 2023). This underscores the necessity of understanding atmospheric NO_3^- dynamics beyond just precursor NO_x emissions, for which ice core NO_3^- can offer invaluable historical perspectives.

In addition to NO_3^- concentrations, its stable isotopic compositions provide valuable information. Nitrogen isotopes ($\delta^{15}N$) differ among NO_x sources and can be used to identify the origin of the NO_3^- (Hastings et al., 2010, 2013). Previous studies of Greenland ice cores have identified decreases in the $\delta^{15}N$ values of NO_3^- ($\delta^{15}N(NO_3^-)$) as early as 1850 CE, which subsequently accelerated after 1950 CE (Hastings et al., 2009; Geng et al., 2014). These decreases in $\delta^{15}N$ have been interpreted as a change in source: increased anthropogenic emissions of NO_x from fossil fuel combustion (Hastings et al., 2009) and/or NO_x derived from soil amended with fertilizer (Felix & Elliott, 2013). In addition, complex factors control $\delta^{15}N(NO_3^-)$. Previous studies have shown that isotopic fractionation can occur during gas–particle partitioning and washout (Freyer, 1991), kinetic NO_2 oxidation (Walters & Michalski, 2015a), and NO_x cycle equilibrium in the atmosphere (Walters et al., 2015b; Walters and Michalski, 2016). Another interpretation of the decrease in $\delta^{15}N$ in ice cores is related to changes in isotopic fractionation between gaseous HNO_3 and particulate NO_3^- that resulted from acidity changes (Geng et al., 2014). The mass-independent oxygen isotope fractionation signals ($\Delta^{17}O = \delta^{17}O - 0.52 \times \delta^{18}O$) of NO_x and NO_3^- can reflect the oxygen source during oxidation (Michalski et al., 2003; Alexander et al., 2009). Positive $\Delta^{17}O$ values of NO_3^- ($\Delta^{17}O(NO_3^-)$) occur as a result of excess ^{17}O (i.e., deviation from mass-dependent fractionation) transferred from O_3 to NO_3^- during photochemical cycling of NO and NO_2 and the oxidation of NO_2 into HNO_3. Thus, mid to high latitudes have $\Delta^{17}O(NO_3^-)$ values of 22–34 ‰ for atmospheric deposition (Michalski et al., 2003, 2012). The $\Delta^{17}O(NO_3^-)$ measurements in ice cores have also been used to investigate historical atmospheric processes (Geng et al., 2017).

However, post-depositional NO_3^- loss in snow/ice can reduce NO_3^- concentrations and change its isotopic compositions (Röthlisberger et al., 2000, 2002; Frey et al., 2009; Akers et al., 2022). Indeed, NO_3^- in snow can undergo photolysis by ultraviolet (UV) light (λ = 290–350 nm, Berhanu et al., 2014), which produces NO_2 that is released into the atmosphere via diffusion or wind pumping. Although NO_2 can partially re-oxidize into NO_3^- in the atmosphere, post-depositional processes can lead to decreases in the NO_3^- concentrations in ice cores (Meusinger et al., 2014; Erbland et al., 2015). In addition, post-depositional processes can also cause significant isotopic fractionation (from −47.9 ‰ to −55.8 ‰) and the remaining NO_3^- becomes enriched in ^{15}N (Berhanu et al., 2015). In contrast, $\Delta^{17}O(NO_3^-)$ is not directly affected by photolysis but instead by the cage effect, in which the intermediate photoproducts (NO_2, NO_2^-, or $ONOO^-$) recombination reactions within snow grains to reform nitrate with exchange with water oxygen or react with radicals (e.g., OH) to regenerate NO_3^- after being emitted to the atmosphere (McCabe et al., 2005; Jiang et al., 2021). The alteration of $\Delta^{17}O(NO_3^-)$ can also occur through the re-oxidation of NO_2 sourced from snow, which leads to nitrate formation in the overlying atmosphere (Erbland et al., 2013). Because NO_3^- photolysis in snow only occurs in the photic zone, the degree of post-depositional alteration is mostly controlled by the snow accumulation rate, as demonstrated in Antarctica (Akers et al., 2022). Even at the Greenland Summit ice core site, the $\delta^{15}N(NO_3^-)$ values of the snowpack are higher than those of the surface snow and the overlying atmosphere (Jarvis et al., 2009; Geng et al., 2014; Fibiger et al., 2016). The Greenland Ice Sheet Project 2 (GISP2) ice core exhibits decreasing $\delta^{15}N(NO_3^-)$ values from glacial to interglacial periods (Hastings et al., 2005; Geng et al., 2015), which has been interpreted as the result of two potential causes: (1) changes in the NO_x source or (2) post-depositional effects related to the snow accumulation rate and dust concentrations. Overall, given the impacts of post-depositional processes, ice core records of NO_3^- and its isotopes require careful consideration.

Accurate understanding of atmospheric NO_3^- and its related nitrogen cycles can be more reliably obtained from ice core records with minimal post-depositional alterations. In this context, the southeastern Dome (SE-Dome) site in Greenland has distinct characteristics, including a snow accumulation rate of 1.01 ± 0.22 m water equivalent per year (m w e a^{-1}) (1960–2014) (Iizuka et al., 2017), which is approximately four times greater than that at the Summit site (0.22 ± 0.05 m w e a^{-1}, Fig.

1c) (Geng et al., 2014). The relatively high accumulation rate is expected to reduce the impact of post-depositional loss, preserving a more representative record of atmospheric NO_3^- deposition. Furthermore, statistical analysis using the Mann–Kendall test for monotonic trends (Kendall, 1975; Mann, 1945) revealed no significant decadal trends in snow accumulation at either the SE-Dome (Kawakami et al., 2023) or the Summit ($p > 0.05$, data from Geng et al. (2014)), suggesting that within-site accumulation variability does not strongly influence nitrate trends at these locations. The Summit and SE-Dome sites receive atmospheric inputs from similar source regions in North America and Western Europe, based on Hybrid Single-Particle Lagrangian Integrated Trajectory (HYSPLIT) 7-day backward trajectory modeling (Figs. 1b and 1c). However, the extent to which post-depositional processes affect NO_3^- isotopic compositions at these sites has not been systematically assessed. In this study, we present the $\delta^{15}N(NO_3^-)$ and $\Delta^{17}O(NO_3^-)$ records obtained from a 90.45 m ice core drilled at the SE-Dome site. By applying the Transfer of Atmospheric Nitrate Stable Isotopes To the Snow (TRANSITS) model (Erbland et al., 2015; Jiang et al., 2021) with site-specific modifications, we evaluate the extent to which post-depositional processes influence NO_3^- at SE-Dome and assess its suitability for reconstructing past atmospheric NO_x emissions. Our results demonstrate that SE-Dome preserves a robust NO_3^- isotopic signal with minimal post-depositional modification, making it a valuable archive for investigating anthropogenic changes in atmospheric NO_3^- over the Northern Hemisphere, particularly from eastern North America and western Europe.

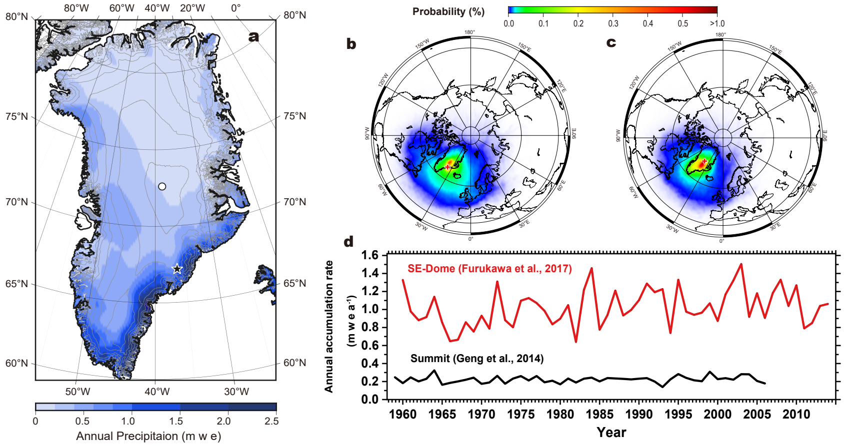

Figure 1. (a) Map of the southeastern Dome (SE-Dome, star) and Summit (opened circle) sites in Greenland (Annual precipitation from ERA5 reanalysis climate data, Hersbach et al., 2020). Probability distributions for the air masses overlying the (b) SE-Dome and (c) Summit sites from 7-day three-dimensional back trajectory analysis based on HYSPLIT modeling (1960–2019). Detailed back trajectory analysis procedures were the same as Iizuka et al. (2018). (d) Annual accumulation rate at the SE-Dome (Furukawa et al., 2017) and Summit (Geng et al., 2014).

2 Materials and Methods

2.1. Samples

This study was based on a 90.45 m ice core drilled at the SE-Dome site in 2015 (67.18° N, 36.37° W, 3170 m a.s.l., Iizuka et al., 2016). The age–depth scale was determined using the oxygen isotope matching method, which matches the $\delta^{18}O$ variations between ice core records and isotope-enabled climate model estimates, and indicated that this ice core covers the period 1959 to 2014 (Furukawa et al., 2017). The reliability of this dating method generally falls within the 95 % confidence interval (typically around an average of ±0.9 months). The greatest uncertainty was reported at 2 months in some years (Furukawa et al., 2017). We divided the ice core samples into four seasons: spring (March 21–June 20), summer (June 21–September 20), autumn (September 21–December 20), and winter (December 21–March 20). For samples analyzed at a two-season resolution (1959–1980 and 1995–2014), spring and summer were combined into summer, whereas autumn and winter were combined into winter. This approach was adopted to ensure a consistent sample size and minimize analytical uncertainty for periods with lower temporal resolution, while still capturing seasonal variations relevant to NO_3^- deposition and atmospheric conditions.

All SE-Dome ice core samples used in this study were stored in a refrigerated room (−50 °C) at the Institute of Low-Temperature Science (Hokkaido University, Sapporo, Japan). Each ice sample (3 × 4 cm cross-dimension) was cut using a band saw in a refrigerated room (−20 °C) and decontaminated by removing the outermost ~5 mm of ice with a ceramic knife in a class 10,000 clean booth, resulting in a loss of approximately 30 % of the original sample weight. The remaining 70 % of the cleaned samples were shipped frozen (~−20 °C) to the Tokyo Institute of Technology (Tokyo Tech, Yokohama, Japan). The samples were then stored in a freezer at −30 °C until analysis.

2.2 Sample analysis

NO_3^- in each sample (n = 136) was separated from other ions using ion chromatography (IC, Dionex Integrion, Thermo Fisher Scientific) according to the methods described by Noro et al. (2018). Changes in the isotopic compositions of NO_3^- during ion chromatographic (IC) separation were <0.4 ‰ for $\delta^{15}N$ values and within the analytical error range for $\Delta^{17}O$ values (Noro et al., 2018). After ion separation, NO_3^- in solution was converted and neutralized to the Na^+ form by passing it through an ion exchange column. The isotopic compositions of NO_3^- were measured using a bacterial method that converts NO_3^- to N_2O (Sigman et al. 2001; McIlvin et al. 2011), followed by N_2O decomposition via microwave-induced plasma (MIP), a technique developed at Tokyo Tech (Hattori et al., 2016). Isotopic reference materials, as well as United States Geological Survey (USGS) standards 32, 34, 35, and their mixtures (prepared in 18.2 MΩ cm water), were also analyzed using the same analytical processes with the samples.

削除: ~~Changes in the isotopic compositions of NO_3^- during ion separation were negligible, as determined previously (Noro et al., 2018).~~ …

Stable isotopic compositions are reported as $\delta X = R_{\text{sample}}/R_{\text{reference}} - 1$, where X denotes ^{15}N, ^{17}O, or ^{18}O, and R denotes the isotope ratios such as $^{15}N/^{14}N$, $^{17}O/^{16}O$, and $^{18}O/^{16}O$, determined for both sample and standard materials. The $\delta^{15}N$, $\delta^{18}O$, and $\Delta^{17}O$ values are reported in permil (‰) notation. The $\delta^{15}N$ values are relative to atmospheric N_2 (air), while the $\delta^{18}O$ and $\Delta^{17}O$ values are relative to Vienna Standard Mean Ocean Water. By propagating the analytical uncertainties for the IC separation and replicating isotopic measurements of USGS standards 34, 35, and 32, the estimated combined uncertainties were ±0.4 ‰ for both $\delta^{15}N(NO_3^-)$ and $\Delta^{17}O(NO_3^-)$.

2.3 TRANSITS modeling

The TRANSITS model (Erbland et al., 2015), a multi-layer 1D isotopic model, was used to simulate NO_3^- recycling across the air–snow interface (i.e., UV photolysis of NO_3^-, NO_x emission, local NO_2 oxidation, and NO_3^- deposition) and its associated isotopic effects. The model is operated at a weekly resolution (52 time steps per year), and the default snow depth resolution is 1 mm. In each step, NO_3^- photolysis is calculated according to the depth-dependent photochemical flux and NO_3^- concentration. All generated NO_2 enters the atmosphere and is re-oxidized to NO_3^-, which is deposited on the surface snow with the primary NO_3^- from long-range transport in the next step. The original snow moves downward as snowfall continues, and newly deposited snow is divided into 1 mm layers. Once the NO_3^- is buried beneath the light transmission band, the layer is regarded as an archive. We adapted the parameters of the TRANSITS model, originally developed for the Summit site by Jiang et al. (2021). This model reproduces the seasonal variation pattern of $\delta^{15}N(NO_3^-)$ in the surface snow at the Summit reported by Jarvis et al. (2009), highlighting the importance of post-depositional processes at the Summit. In addition, this model estimated the net loss of NO_3^- (4.1 %) and associated changes in $\delta^{15}N(NO_3^-)$ (+2.6 ‰) and $\Delta^{17}O(NO_3^-)$ (–0.9 ‰) between primary deposition and NO_3^- archived in the ice, under an estimate of the horizontal export fraction of locally re-oxidized NO_3^- (f_{exp}) of 35% (Jiang et al., 2021). In this study, we applied the same model under the SE-Dome condition by adjusting the parameters to examine the effects of snow NO_3^- photolysis on NO_3^- concentration and its isotopes.

The snow accumulation rate was set at 1.01 m w e a^{-1}, based on the 1960–2014 average from SE-Dome ice core data (Iizuka et al., 2017), with additional tests conducted at rates of 0.25, 0.6, and 1.4 m w e a^{-1}. The mass balance of NO_3^- between the snow and atmosphere depends on NO_3^- influxes and outfluxes. We expressed the NO_3^- flux as F_Y, which includes the primary NO_3^- flux from long-range transport (F_{pri}), NO_3^- flux from NO_3^- photolysis (F_P), atmospheric NO_3^- deposition flux (F_D), and ice-core NO_3^- flux buried beneath the light band (F_A). These fluxes reflect changes in NO_3^- and its isotopic compositions in the snow and atmosphere. The TRANSITS model considers that two processes can change $\delta^{15}N(NO_3^-)$ as a result of isotope fractionation from UV photolysis and NO_3^- deposition (i.e., co-condensation and dry deposition). The nitrogen isotope fractionation constant during photolysis ($^{15}\varepsilon_p$) was calculated using a ratio of $^{14}NO_3^-$ and $^{15}NO_3^-$ photolysis rates ($^{15}\varepsilon_p = {}^{15}J/{}^{14}J - 1$, where J represents the photolysis rate constant) in each snow layer (Erbland et al., 2013). The J at different depths (z) ($J(z)$) was calculated according to Equation (1):

$$J(z) = \int_{280nm}^{350nm} \Phi(\lambda)\times\sigma_{NO_3^-}(\lambda)\times I\,(z, \lambda)\,d\lambda, \qquad (1)$$

where I is the actinic flux and Φ and σ are the quantum yield and absorption cross-section of NO_3^- photolysis, respectively. The quantum yield of NO_3^- photolysis has significant uncertainties (Meusinger et al., 2014). However, it is unlikely that the quantum yield of NO_3^- photolysis would differ substantially between the SE-Dome and Summit sites. Since this study compares the differences between these sites, which have notably different snow accumulation rates, the quantum yield of NO_3^- photolysis at the SE-Dome site was set to the same value (0.002) as that estimated for the Greenland Summit site by Jiang et al. (2021). The absorption cross sections of $^{14}NO_3^-$ ($^{14}\sigma_{NO3-}$) and $^{15}NO_3^-$ ($^{15}\sigma_{NO3-}$) were derived from Berhanu et al. (2014). The nitrogen isotope fractionation constant during deposition ($^{15}\varepsilon_d$) was set to +10 ‰ (Erbland et al., 2015). For the oxygen isotopes, only the mass-independent fractionation signal ($\Delta^{17}O$) was modeled. The cage effect (i.e., decrease in $\Delta^{17}O$ of the snow NO_3^- owing to secondary chemistry during NO_3^- photolysis, McCabe et al., 2005) was set to 15 % according to Erbland et al. (2015), and the TRANSITS model calculated the exchange of oxygen atoms with water during UV photolysis and atmospheric NO–NO_2 cycling, both of which alter $\Delta^{17}O$. The $\Delta^{17}O(NO_3^-)$ fractionation mechanisms in the TRANSITS model during these processes are explained in detail in Jiang et al. (2021).

The atmospheric boundary layer at the SE-Dome site was assumed to be a zero-dimensional well-mixed box, and the snowpack was assumed to be a stack of snow layers deposited at different times. Weekly air temperatures (T), pressures (P), and average boundary layer heights (h) from 1950–2020 were obtained from the second-generation European Centre for Medium-Range Weather Forecast atmospheric analysis of global climate (ERA5) (Hersbach et al., 2020; Khalzan et al., 2022). O_3, OH, peroxyl radical (RO_2 and HO_2), and BrO concentrations were used to calculate the rates of NO–NO_2 cycling and NO_2 oxidation to HNO_3. However, because these records were not available for the SE-Dome, they were extracted from the outputs of the v.12.9.3 (https://zenodo.org/records/3959279, last accessed: 7 Jan 2024) GEOS-Chem atmospheric chemical transport model (http://www.geos-chem.org, last accessed: 7 Jan 2024) using the Modern-Era Retrospective analysis for Research and Applications, Version 2 (MERRA-2) meteorological field, with 4° latitudinal and 5° longitudinal resolutions. The GEOS-Chem model was run for year 2017 after a one-year spin up run, and the monthly averages for the O_3, OH, HO_2, and BrO concentrations in the planetary boundary layer in the SE-Dome grid were used. We selected 2017 as the representative period, which should not vary significantly from other recent years and should ensure robust outcomes. Given that tropospheric O_3 concentrations were comparable between the SE-Dome and Summit grids in the GEOS-Chem model, the total O_3 column (TCO) was set to the same (266 to 408 DU) as that used in a previous study of the Summit site (Jiang et al., 2021). F_{pri} was estimated to be 16.4, 23.6, 13.3, 11.5 mg-N m^{-2} a^{-1} for spring, summer, fall and winter respectively, based on the seasonal NO_3^- fluxes at the SE-Dome site from 1960 to 2014 (Iizuka et al., 2018).

An e-folding depth, which is the depth to which light enters the snow layer and attenuates to an initial intensity of 1/e (owing to absorption and scattering), for the SE-Dome site was calculated using the snow density (ρ_{snow}), the calculated specific surface area (SSA), and fixed light-absorbing impurity concentrations (Jiang et al., 2021). The ρ_{snow} of 400 kg m^{-3} for the SE-Dome site was obtained from an observation at the SE-Dome (Oyabu et al., 2016). The SSA for the SE-Dome site was determined to be 47.0 m^2 kg^{-1} using the relationship between the SSA and ρ_{snow}, according to a previous study (Domine et al., 2007) as follows:

$$SSA = -174.13 \times \ln(\rho_{snow}) + 306.4, \qquad (2)$$

where SSA is in units of cm^2 g^{-1} and the units for ρ_{snow} was changed to g cm^{-3}. For the light-absorbing impurity concentrations, we established constant concentrations of the three main light-absorbing impurities in snow: dust, soot (BC), and organic humic-like substances (HULIS). The dust concentration was set to 33.94 ng g^{-1} according to an average concentration for the SE-Dome ice core from 1960–2014 (Amino et al., 2021). Owing to a lack of direct observations for BC and HULIS at the SE-Dome, we assumed these concentrations based on the Ca^{2+} concentration ratio between the Summit and SE-Dome sites. Here, $[\mathrm{BC}]_{\mathrm{Summit}}$ and $[\mathrm{HULIS}]_{\mathrm{Summit}}$ were set to 1.4 and 31 ng g^{-1}, respectively, according to Jiang et al. (2021). Furthermore, [Ca^{2+}] at the Summit site was set to 6.5 ng g^{-1} according to an average of 2 m shallow snow pack observation (Geng et al., 2014); [Ca^{2+}] at the SE-Dome site was set to 11.6 ng g^{-1} according to an average from the SE-Dome ice core from 1960–2014 (Iizuka et al., 2018). Thus, $[\mathrm{BC}]_{\mathrm{SE\text{-}Dome}}$ and $[\mathrm{HULIS}]_{\mathrm{SE\text{-}Dome}}$ were calculated as 2.2 and 47.6 ng g^{-1}, respectively, and used for the model calculation. An e-folding depth of 10 cm was obtained based on the above inputs. The calculated e-folding depth for the SE-Dome site was consistent with previous estimates from the GEOS-Chem model investigating the impact of post-depositional effect in snow (Zatko et al., 2016).

The horizontal export fraction of locally re-oxidized $\mathrm{NO_3^-}$ (f_{exp}) under the SE-Dome condition was calculated with the same scheme described for the Antarctic Plateau (Erbland et al., 2015) and Greenland Summit (Jiang et al., 2021), as following equations.

$$f_{\mathrm{exp}}=\frac{\frac{1}{\tau_1}}{\frac{1}{\tau_1}+\frac{1}{\tau_2}}\times\left(1+\frac{\frac{1}{\tau_2}}{\frac{1}{\tau_3}+\frac{1}{\tau_1}}\right) \tag{3}$$

$$\tau_1=\frac{L}{V_{\mathrm{h}}} \tag{4}$$

$$\tau_2=\frac{1}{k[\mathrm{OH}]} \tag{5}$$

$$\tau_3=\frac{H}{V_{\mathrm{d}}} \tag{6}$$

In these equations, τ_1, τ_2, and τ_3 represent the lifetimes of horizontal transport, oxidation of $\mathrm{NO_2}$ by OH radicals, and vertical deposition, respectively. L and H denote the summer boundary layer height and horizontal characteristic, while V_{h} is the mean horizontal wind speed, k is the rate constant for the $\mathrm{NO_2}$ + OH reaction, and V_{d} is the dry deposition velocity of $\mathrm{HNO_3}$ (Jiang et al., 2021). The values used for the calculation are summarized in Table S2, and the same physicochemical values as those of Summit were used, while parameters such as temperature and boundary layer height were incorporated from ERA5 data. We obtained f_{exp} to be 47% under the SE-Dome condition, but the calculated f_{exp} may oversimplify the processes governing $\mathrm{NO_3^-}$ deposition and the chemical loss pathways of NO_x as discussed previously (Jiang et al., 2021). Therefore, we considered the sensitivity of post-depositional alteration to variations in f_{exp} between initial deposition and the point at which $\mathrm{NO_3^-}$ becomes archived in the ice. Therefore, we considered the sensitivity of post-depositional alteration to variations in f_{exp} between initial deposition of $\mathrm{NO_3^-}$ and its permanently archived in the ice.

At the initial time (t = 0) in the TRANSITS model, the $\mathrm{NO_3^-}$ concentration was set to 71.12 ng g^{-1} based on the average $\mathrm{NO_3^-}$ concentration in the SE-Dome I ice core (Iizuka et al., 2018), while the $\delta^{15}\mathrm{N(NO_3^-)}$ and $\Delta^{17}\mathrm{O(NO_3^-)}$ values in the snowpack were set to 0 ‰ and 30 ‰, respectively, according to previous TRANSITS settings (Erbland et al., 2015; Jiang et al., 2021). This initial isotopic parameter does not affect the model interpretation of changes in $\delta^{15}\mathrm{N(NO_3^-)}$ and $\Delta^{17}\mathrm{O(NO_3^-)}$ due to post-depositional processing. Three-year distributions of $\mathrm{NO_3^-}$ and its isotopes were simulated with and without $\mathrm{NO_3^-}$ photolysis scenarios under the SE-Dome condition, from which profiles of $\mathrm{NO_3^-}$ concentrations, $\delta^{15}\mathrm{N(NO_3^-)}$, and $\Delta^{17}\mathrm{O(NO_3^-)}$ were output. The parameters used in the TRANSITS model are summarized in Table 1 and Supplement data file 1.

2.4 Statistical analysis

XLSTAT 2023 (Addinsoft, Paris, France) was used for the Mann–Kendall trend analysis over 1959–2014. SPSS 25 (IBM SPSS, Armonk, NY, USA) was used to perform the *t*-tests of annual changes in $\delta^{15}N(NO_3^-)$ and NO_3^- concentrations. Statistical significance was set at $p < 0.05$.

3 Results

3.1 Nitrate isotope records from the SE-Dome ice core

The NO_3^- isotope data and fluxes obtained from the SE-Dome ice core are shown in Figs. 2 and S1. The seasonal variations were larger in the samples analyzed at a four-season resolution (1981–1994), which may have been caused by age errors (Furukawa et al., 2017). Accordingly, mass-weighted averages were calculated for the summer and winter fractions from the seasonal samples during 1981–1994. From 1959 to 2014, the $\delta^{15}N(NO_3^-)$ values were generally higher in summer (−2.9 ± 2.6 ‰) than in winter (−6.9 ± 2.9 ‰) (Figs. 2a and S1a). To assess annual changes in $\delta^{15}N(NO_3^-)$ over this period, we calculated the annual mass-weighted average $\delta^{15}N(NO_3^-)$ values and found that they decreased from 1959 to 1974 and exhibited no significant ($p > 0.05$) trends after 1975 (mean value of −4.8 ± 1.3 ‰) (Fig. 2a). No clear relationship was observed between the annual variations in $\delta^{15}N(NO_3^-)$ and NO_3^- concentrations ($p = 0.37$).

Using a similar method as for $\delta^{15}N(NO_3^-)$, we also calculated the mass-weighted average and annual mass-weighted average for $\Delta^{17}O(NO_3^-)$. $\Delta^{17}O(NO_3^-)$ also exhibited a seasonal pattern, with lower values in the summer (27.8 ± 1.3 ‰) than those in the winter (31.3 ± 1.9 ‰), yielding a mass-weighted average of 29.3 ± 1.2 ‰ over the entire period (Figs. 2b and S1). The average annual $\Delta^{17}O(NO_3^-)$ values were relatively high (~33 ‰) in 1988, and low values were observed in 2013 and 2014 (Fig. 2b). Excluding these particular years, no significant annual increases or decreases ($p > 0.05$) were observed in the $\Delta^{17}O(NO_3^-)$ values.

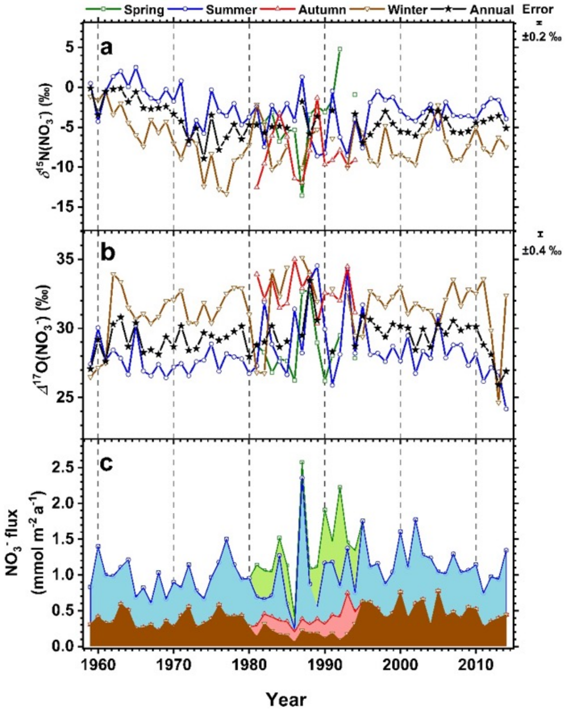

Figure 2. NO_3^- isotope data and fluxes from the SE-Dome ice core. (a) $\delta^{15}N(NO_3^-)$, (b) $\Delta^{17}O(NO_3^-)$, and (c) NO_3^- flux (mmol m^{-2} a^{-1}).

3.2 TRANSITS model results

We aimed to know the changes in NO_3^- from primary deposition to the ice core archive. However, these changes primarily depend on the f_{exp} value—the fraction of NO_3^- exported from the site of photolysis. Therefore, we calculated the dependency of the $\delta^{15}N(NO_3^-)$ and $\Delta^{17}O(NO_3^-)$ values on f_{exp} at the SE-Dome using the same approach as Jiang et al. (2021) (Fig. 3). The post-depositional alterations in $\delta^{15}N(NO_3^-)$ and $\Delta^{17}O(NO_3^-)$ between initial deposition and ice-core NO_3^- concentration at the SE-Dome were dependent on f_{exp}. As shown in Fig. 3, an inverse relationship was observed between f_{exp} and $\delta^{15}N(NO_3^-)$ and $\Delta^{17}O(NO_3^-)$. In the case of $\delta^{15}N$, when f_{exp} is high, a larger proportion of isotopically light NO_3^- is removed from the snowpack due to strong isotopic fractionation during photolysis. As a result, the remaining NO_3^- in the snow becomes isotopically enriched in ^{15}N. In contrast, for $\Delta^{17}O(NO_3^-)$, when f_{exp} is high, the impact of photolysis-induced isotopic fractionation on $\Delta^{17}O(NO_3^-)$ is minimal, and thus, its value remains largely unchanged. Conversely, when f_{exp} is low (i.e., a significant portion of nitrogen species is emitted and subsequently redeposited), the NO_3^- with lower $\Delta^{17}O(NO_3^-)$, originating from NO_2 + OH reaction, dominates the signal, leading to a decrease in $\Delta^{17}O(NO_3^-)$. These distinct mechanisms explain why $\delta^{15}N(NO_3^-)$ and $\Delta^{17}O(NO_3^-)$ exhibit opposite trends.

However, the degree to which the changes in δ^{15}N(NO$_3^-$) and Δ^{17}O(NO$_3^-$) were dependent on f_{exp} was less evident at the SE-Dome than at the Summit (Fig. 3). Notably, even when the snow accumulation rate for SE-Dome is adjusted from the minimum (0.6 m w e a^{-1}) to the maximum (1.4 m w e a^{-1}) values, as shown in Fig. 1d, the results indicate that changes in δ^{15}N(NO$_3^-$) and Δ^{17}O(NO$_3^-$) are less sensitive to f_{exp} compared to Summit. Furthermore, when a snow accumulation rate of 0.25 m w.e. a^{-1}, equivalent to that used in the Summit study (Jiang et al., 2021), was applied, the variations were nearly identical to those observed at Summit (Fig. S2). This suggests that the differences in post-depositional alterations for δ^{15}N(NO$_3^-$) and Δ^{17}O(NO$_3^-$) are primarily caused by differences in accumulation rates.

Using the method of Erbland et al. (2015), f_{exp} was calculated as 47 % at the SE-Dome, reflecting an estimated net loss of 1.4 % due to post-depositional alteration in NO$_3^-$ concentration at the SE-Dome, with corresponding changes in δ^{15}N(NO$_3^-$) and Δ^{17}O(NO$_3^-$) of +0.9 ‰ and −0.2 ‰, respectively (Fig. 3). In contrast, the estimated net loss of NO$_3^-$ under the Summit condition showed greater net loss in NO$_3^-$ (4.1 %) and associated changes in δ^{15}N(NO$_3^-$) (+2.6 ‰) and Δ^{17}O(NO$_3^-$) (−0.9 ‰) when f_{exp} value is 35 % estimated previously (Jiang et al., 2021). Thus, even when using the same evaluation criteria, the post-depositional alteration in NO$_3^-$ and its isotopic compositions at the SE-Dome were smaller than those at the Summit. We note that, at an extreme condition of f_{exp} = 100 %, the estimated changes in δ^{15}N(NO$_3^-$) from initial deposition due to post-depositional processing under the SE-Dome condition were +1.8 ‰, which is significantly lower than that under the Summit condition of +6.8 ‰ (Fig. 3).

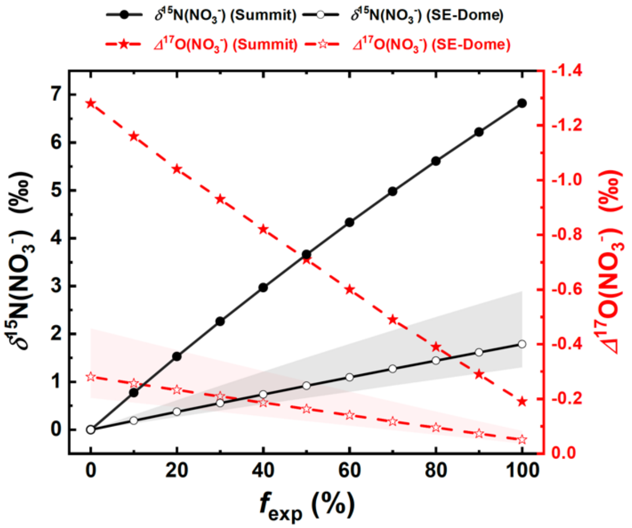

Figure 3. Sensitivity of the changes in δ^{15}N(NO$_3^-$) and Δ^{17}O(NO$_3^-$) of the ice-core nitrate to f_{exp}. Positive/negative values indicate deviations from initial deposition. The shaded area in the SE-Dome calculations represents results obtained using snow accumulation rates of 0.6 and 1.4 m w e a^{-1}.

Figure 4 shows the results obtained from the TRANSITS model for NO$_3^-$ and its isotopic compositions for the SE-Dome site with considering f_{exp} value of 47%. The model considering photolysis showed a maximum 6 % decrease in the annual NO$_3^-$ concentrations during spring and early summer compared to the scenario without photolysis (Fig. 4a). The post-depositional effects (primarily due to photolytic isotopic fractionation) caused a fluctuation from −1 to +2 ‰ in δ^{15}N(NO$_3^-$), with higher values in summer (1.3 ± 0.7 ‰) and lower values in winter (0.2 ± 0.2 ‰) (Fig. 4b). The variation in the Δ^{17}O(NO$_3^-$) value, which was initially set at 30 ‰, is attributed to a slight decrease in atmospheric NO_3^- concentration owing to its re-oxidization during spring to summer. Thus, when photolysis is minimal in the autumn and winter, the $\Delta^{17}O(NO_3^-)$ values remained close to the initial value (30 ‰) (Fig. 4c). Conversely, during spring and summer, when $\delta^{15}N(NO_3^-)$ values increase, a decreasing $\Delta^{17}O(NO_3^-)$ trend was observed (Fig. 4c). However, the extent of this change is minimal, with values reaching a minimum of ~29.6 ‰. The seasonality in NO_3^- concentration and post-depositional alteration in its isotopic composition were less obvious at the SE-Dome than that at the Summit, where $\delta^{15}N(NO_3^-)$ varied by >5 ‰ and $\Delta^{17}O(NO_3^-)$ by ~2 ‰ (Jiang et al., 2021).

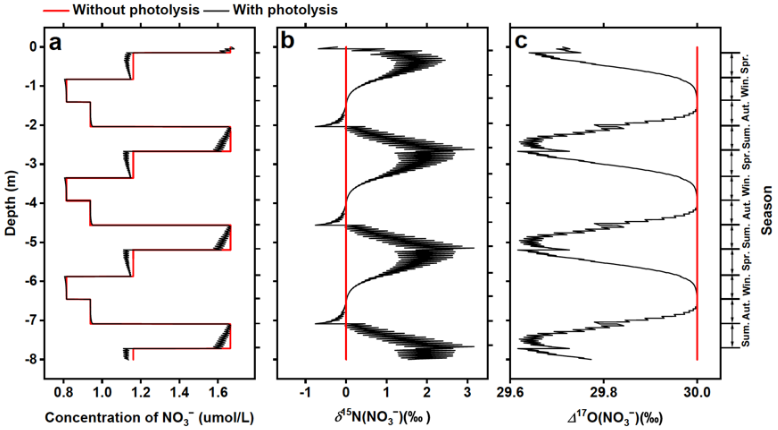

Figure 4. TRANSITS model results for the SE-Dome site. (a) NO_3^- concentration, (b) $\delta^{15}N(NO_3^-)$, and (c) $\Delta^{17}O(NO_3^-)$. The black and red lines represent the variations calculated without and with NO_3^- photolysis, respectively.

4 Discussion

4.1 $\delta^{15}N(NO_3^-)$ values from the SE-Dome and Summit sites

Figure 5 shows the annual average $\delta^{15}N(NO_3^-)$ values obtained from the SE-Dome ice core and the previously published $\delta^{15}N(NO_3^-)$ values from the Summit site (Hastings et al., 2009; Geng et al., 2014). Decreasing trends in $\delta^{15}N(NO_3^-)$ were observed in both the Summit and SE-Dome ice cores until approximately 1974, after which no clear changes occurred (Fig. 5). Notably, based on the overlapping analysis period from 1959 to 2006 (n = 44), the annual $\delta^{15}N(NO_3^-)$ values in the SE-Dome ice core were found to be 4.2 ± 2.8 ‰ lower than those in the Summit ice core (Fig. 5). The observed differences in $\delta^{15}N(NO_3^-)$ values between the SE-Dome and Summit may be attributed to (1) variations in the $\delta^{15}N$ values of NO_3^- deposited at the two sites and/or (2) variations in the degree of post-depositional alterations between the two sites. These two points are discussed in detail below.

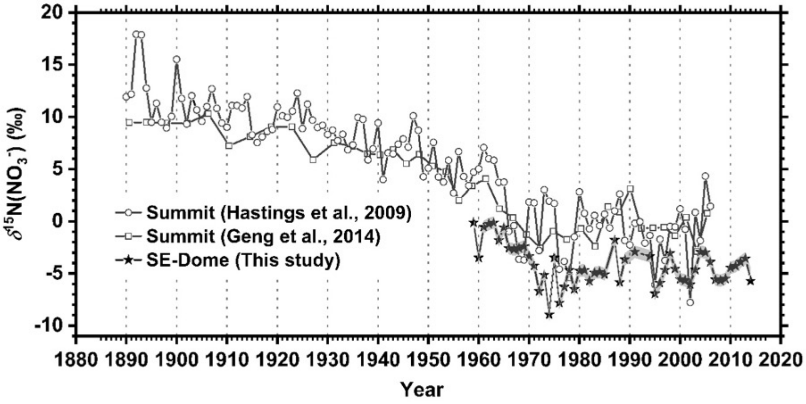

Figure 5. $\delta^{15}N(NO_3^-)$ values obtained from the SE-Dome (this study) and Summit (Hastings et al., 2009; Geng et al., 2014) ice cores. The shaded area for $\delta^{15}N(NO_3^-)$ values in SE-Dome represents the propagated errors of the annual average, based on seasonal concentration and $\delta^{15}N$ variations.

First, regarding the differences in the $\delta^{15}N$ values of NO_3^- deposited at the two sites, there are two main sources for the NO_3^- deposited in the Greenland ice core. One long-range source is derived primarily from anthropogenic sources outside of Greenland. The other source involves NO_x released from NO_3^- photolysis within the snowpack, which is then re-oxidized and redeposited. Although the air masses at the SE-Dome and Summit sites have similar source regions—North America and Western Europe (Figs. 1b and 1c)—the degree of influence from reactive nitrogen sources differed between sites (Fig. S3). At the SE-Dome, the contributions from outside Greenland were relatively high, with nearly equal influence from North America and EU countries (Fig. S3b). In contrast, the contributions from EU countries were relatively low at the Summit, while the North American countries (mostly Eastern Canada) and inner Greenland had greater contributions (Fig. S3c). NO_x sources from Western Europe and North America are not necessarily similar; for example, differences in the relative contributions of various NO_x sources are reflected in their $\delta^{15}N$ values, with NO_x from coal and biomass tending to have higher $\delta^{15}N$ values, while NO_x from oil, natural gas, and soil tends to have lower $\delta^{15}N$ values (e.g., Elliot et al., 2019). To date, there have been no studies comprehensively comparing the isotopic composition of atmospheric NO_3^- between Europe and North America. The limited available data shows that $\delta^{15}N$ values in total atmospheric NO_3^- (sum of gaseous HNO_3 and particulate NO_3^-) at the northeast US range −10 to +5 ‰ (Bekker et al., 2023), while those in rainwater NO_3^- (including both gaseous HNO_3 and particulate NO_3^-) in Switzerland range −12 to +6 ‰ (Freyer, 1991), which cannot be distinguished from each other. A recent study (Song et al., 2021) compiled the δ^{15}N values of precipitated NO_3^- between urban and non-urban areas in Europe ($n = 8$ and $n = 15$, respectively) and North America ($n = 10$ and $n = 73$, respectively), showing no clear distinction between the two regions, though Europe exhibited slightly higher values. Hence, there is no clear evidence that the long-term δ^{15}N trends in European countries consistently remain lower than those in the USA or Canada, and thus, the ~4‰ lower $\delta^{15}N(NO_3^-)$ values observed in the SE-Dome, which is relatively more influenced by air masses from Europe, cannot be explained solely by differences in air mass origin.

Considering the potential impact of snow-sourced NO_x and re-oxidized NO_3^-, it is important to note that the extent of recycled NO_x from NO_3^- photolysis in the Greenland ice sheet differed between these two sites. As modeled by Zatko et al. (2016), recycled NO_x is typically more important at inland sites such as the Summit than coastal sites such as the SE-Dome. Additionally, the contribution of air masses from inside Greenland was higher at the Summit than at the SE-Dome (Fig. S3). Nevertheless, the δ^{15}N values of NO_x and re-oxidized NO_3^- are typically low due to isotopic fractionation during snow NO_3^- photolysis in the snow and ice, with $\delta^{15}N(NO_3^-)$ in high-latitude air masses attributed to photochemical NO_x production in snow, resulting in $\delta^{15}N(NO_3^-)$ values of −10 to −43 ‰ in polar regions (e.g., Savarino et al., 2007; Morin et al., 2009; Shi et al., 2021). Thus, the contribution of locally recycled NO_3^-, which was greater at the Summit, cannot explain why $\delta^{15}N(NO_3^-)$ values were lower at the SE-Dome than at the Summit.

Finally, regarding the differences in post-depositional alterations between two sites, we applied parameters specific to the SE-Dome in the TRANSITS model (Figs. 3 and 4). The model results for the SE-Dome, accounting for post-depositional NO_3^- photolysis, showed a net NO_3^- loss of 1.3 % and increase of +0.9 ‰ in $\delta^{15}N(NO_3^-)$ (see Section 3.2). In comparison, the Summit condition resulted in a ~4 % net NO_3^- loss and +2.6 ‰ increase in $\delta^{15}N(NO_3^-)$ (Jiang et al., 2021). Although the lower $\delta^{15}N(NO_3^-)$ values at the SE-Dome can be partially explained by the model, they cannot be fully accounted for quantitatively. However, the estimated +2.6 ‰ increase in $\delta^{15}N(NO_3^-)$ at the Summit may be underestimated due to an underestimation in f_{exp} (Jiang et al., 2021). Indeed, an observational study (Honrath et al., 2002) indicates that most of the NO_x and/or HNO_3 emitted from the snow at Summit is largely exported from the local boundary layer if no wet deposition occurs, suggesting that the f_{exp} value can reach ~1 under Summit conditions. Therefore, the actual net NO_3^- loss and $\delta^{15}N(NO_3^-)$ variation at the Summit may have been larger than the 4 % estimated by Jiang et al. (2021). Thus, when considering higher f_{exp} values, the difference due to post-depositional alterations could be higher than the modeled difference between the SE-Dome (+0.9 ‰, this study) and Summit (+2.6 ‰, Jiang et al., 2021). Indeed, when considering an extreme condition of $f_{exp} = 100$ %, the difference between the Summit and SE-Dome becomes ~5 ‰ (Fig. 3). Overall, although there is some uncertainty in the model, it is likely that the SE-Dome experienced less post-depositional alteration, thus preserving the atmospheric $\delta^{15}N(NO_3^-)$ values more effectively than at the Summit.

Although the contribution of different NO_3^- sources cannot be entirely ruled out, our analysis shows that the observed $\delta^{15}N(NO_3^-)$ value at SE-Dome, which is 4.2 ± 2.8‰ lower than that at Summit, can largely be attributed to differences in post-depositional alterations.

4.2 Seasonal variations in NO_3^- isotopes

The post-depositional effect, as estimated from the TRANSITS model, yielded a summer-winter difference in $\delta^{15}N(NO_3^-)$ of 1.1 ± 0.7 ‰ and a difference smaller than 0.5 ‰ in $\Delta^{17}O(NO_3^-)$, as described in Section 3.2 (Figs. 4b and 4c). In contrast, except for the anomalous years (1959–1961, 1972, 1995, 2005, and 2013), the observed summer–winter differences for respective years in the SE-Dome ice core were 5.3 ± 2.4 ‰ (0.4–9.8 ‰) for $\delta^{15}N(NO_3^-)$ and −4.2 ± 1.5 ‰ (from −8.2 to −0.4 ‰) for $\Delta^{17}O(NO_3^-)$, respectively (Figs. 2a and 2b), which were larger than the differences estimated by the TRANSITS model. Thus, the observed differences between the summer and winter NO_3^- isotopes were not solely explained by post-depositional alteration. Consequently, seasonal differences in $\delta^{15}N(NO_3^-)$ and $\Delta^{17}O(NO_3^-)$ likely reflect atmospheric changes.

The observed seasonal $\delta^{15}N(NO_3^-)$ trend (high in summer and low in winter) at the SE-Dome site was consistent with observations made at two coastal Arctic sites (Morin et al., 2008, 2012) but inconsistent with typical seasonal $\delta^{15}N(NO_3^-)$ values of aerosols in mid-latitude regions that are high in winter and low in summer (Freyer, 1991; Freyer et al., 1996; Lim et al., 2022). Although the specific process has yet to be identified, the factors controlling high $\delta^{15}N(NO_3^-)$ values in the summer have been comprehensively reviewed (Jiang et al., 2024 and references therein). One possibility is that physicochemical transformations of $\mathrm{NO_3^-}$ related to temperature influence $\delta^{15}\mathrm{N}(\mathrm{NO_3^-})$ values, as suggested by a strong correlation between high $\delta^{15}\mathrm{N}(\mathrm{NO_3^-})$ values and summer air temperatures (Morin et al., 2008). Another possibility is the incursion of anthropogenic sources, as proposed by Morin et al. (2009), which is supported by indicates that air parcels originating from regions with greater anthropogenic influence carry higher $\delta^{15}\mathrm{N}(\mathrm{NO_3^-})$ values. This is supported by observational studies on atmospheric $\delta^{15}\mathrm{N}(\mathrm{NO_3^-})$ (e.g., Vicars and Savarino, 2014) and the increased frequency of air masses originating from North America during summer compared to winter (Kahl et al., 1997). While definitive conclusions regarding these observations have not yet been determined, it is hypothesized that the observations may be influenced by a combination of factors, including NO_x sources, gas–particle partitioning variability influenced by temperature (Freyer, 1991) and acidity (Geng et al., 2014), oxidation pathways (Walters et al., 2016), and differences in transport efficiency and removal processes (Heaton, 1987; Beyn et al., 2014). Future studies should examine the differences in $\delta^{15}\mathrm{N}(\mathrm{NO_3^-})$ variations between both the source and remote regions. Such comparative analyses could enhance the current understanding of the underlying processes that influence isotopic compositions in different geographical contexts.

The observed seasonal changes in $\Delta^{17}\mathrm{O}(\mathrm{NO_3^-})$ (high in winter and low in summer, Fig. 2b) were consistent with typical seasonal variations in $\Delta^{17}\mathrm{O}(\mathrm{NO_3^-})$ (e.g., Michalski et al., 2003). In summer, increased sunlight promotes the formation of $\mathrm{HNO_3}$ via $\mathrm{NO_2}$ + OH reactions, leading to lower $\Delta^{17}\mathrm{O}(\mathrm{NO_3^-})$ values. Conversely, in winter, $\mathrm{N_2O_5}$ hydrolytic or $\mathrm{NO_3}$ radical pathways forming $\mathrm{HNO_3}$ in the presence of $\mathrm{O_3}$ predominate and result in increased $\Delta^{17}\mathrm{O}(\mathrm{NO_3^-})$ levels. Although this kind of seasonal variation in $\Delta^{17}\mathrm{O}(\mathrm{NO_3^-})$ is well known, we confirmed the historic occurrence of similar seasonal variations in the atmosphere. Although the scope of the current study limits further discussion in this regard, future research should explore the differences in $\Delta^{17}\mathrm{O}(\mathrm{NO_3^-})$ between summer and winter during the preindustrial period when anthropogenic contributions of $\mathrm{NO_3^-}$ were significantly lower.

4.3 Decadal variations in $\mathrm{NO_3^-}$ isotopes

As discussed in Section 4.1, the SE-Dome ice core recorded atmospheric $\mathrm{NO_3^-}$ deposition with minimal post-depositional effects. The decadal $\delta^{15}\mathrm{N}(\mathrm{NO_3^-})$ trend obtained from ice cores in Greenland has been interpreted to indicate changes in the NO_x source (Hastings et al., 2009) and/or atmospheric acidity from the beginning of the Industrial Revolution to the present (Geng et al., 2014). In response to emission controls since 1975, reasonable changes in dominant NO_x emissions and the adoption of NO_x removal technology such as three-way catalytic converters are expected, which can affect the $\delta^{15}\mathrm{N}(\mathrm{NO_3^-})$ values (e.g., Walters et al. 2015). As for acidity, if $\delta^{15}\mathrm{N}(\mathrm{NO_3^-})$ is primarily controlled by atmospheric acidity, as proposed by Geng et al. (2014), $\delta^{15}\mathrm{N}(\mathrm{NO_3^-})$ should have increased after approximately 1975 when the atmospheric acidity decreased (owing to $\mathrm{SO_2}$ emission controls, Hattori et al., 2021). However, the $\delta^{15}\mathrm{N}(\mathrm{NO_3^-})$ values obtained herein did not increase until 2014, indicating that there are multiple factors controlling ice core $\delta^{15}\mathrm{N}(\mathrm{NO_3^-})$ values. As this study only covers a relatively limited period (60 years), future studies should address and compare longer ice core records from different regions. Such comparisons would be beneficial for understanding the factors behind isotopic variations, thereby enabling more accurate interpretations of isotopic records reconstructed from ice cores.

The unusually high $\mathrm{NO_3^-}$ fluxes observed in the summer of 1987 (1.97 mmol $\mathrm{m^{-2}\ a^{-1}}$) and the spring of 1992 (1.38 mmol $\mathrm{m^{-2}\ a^{-1}}$) were also notable (Fig. 2c). The extent of forest fires in North America can be the primary driver of this phenomenon, based on coincident high $\mathrm{NH_4^+}$ fluxes during these periods (Iizuka et al., 2018). In 1992, the Mt. Pinatubo eruption may have influenced the observations, considering the high $\mathrm{SO_4^{2-}}$ concentration (13.7 µmol $\mathrm{L^{-1}}$, Iizuka et al., 2018). The $\delta^{15}\mathrm{N}(\mathrm{NO_3^-})$ values during the summer of 1987 (1.3 ‰) and the spring of 1992 (4.8 ‰) were relatively high compared with other years during which $\delta^{15}\mathrm{N}(\mathrm{NO_3^-})$ was less than 0 ‰. These higher $\delta^{15}\mathrm{N}(\mathrm{NO_3^-})$ values may be related to biomass burning associated with forest fires (−4.3 ‰ to +7.0 ‰, Chai et al., 2019). Stratospheric $\mathrm{NO_3^-}$ inputs may also have high $\delta^{15}\mathrm{N}$ values, as observed in Antarctic aerosols (Savarino et al., 2007). However, the $\Delta^{17}\mathrm{O}(\mathrm{NO_3^-})$ values in the summer of 1987 (28.2 ‰) and the spring of 1992 (29.5 ‰) were not clearly different from other years, which is not consistent with high $\Delta^{17}\mathrm{O}(\mathrm{NO_3^-})$ trend during pre-industrial biomass-burning (i.e., forest fires) reported in the previous study (Alexander et al., 2004). We also note that no biomass burning tracers were detected both in 1987 and 1992 (Parvin et al., 2019). Further research is therefore required to link nitrate isotopes with specific events such as biomass burning.

The $\Delta^{17}O(NO_3^-)$ record from the SE-Dome core did not exhibit clear trends during the past 60 years. During this period, changes in atmospheric oxidants have occurred, such as increases in tropospheric O_3 over Arctic regions (Law et al., 2023). It is reasonable to estimate that higher O_3 can induce increases in $\Delta^{17}O(NO_3^-)$ by: (1) promoting NO_2 formation from NO + O_3 reactions and (2) promoting NO_2 oxidation to NO_3 (and subsequently to HNO_3) by O_3. However, such changes were not recorded in the $\Delta^{17}O(NO_3^-)$ data from the SE-Dome ice core. During this period, atmospheric sulfate formation was changed by the promotion of in-cloud S(IV) + O_3 reactions, based on increases in $\Delta^{17}O(SO_4^{2-})$ from the same SE-Dome ice core (Hattori et al., 2021). Thus, further research is required to determine the mechanism(s) behind the observed constant $\Delta^{17}O(NO_3^-)$ values in ice cores after emission controls by comparing $\Delta^{17}O(NO_3^-)$ values estimated using chemical transport models such as GEOS-Chem (Alexander et al. 2009; Alexander et al. 2020). Based on the $\Delta^{17}O(NO_3^-)$ values recorded in the GISP2 ice core, the variations have been attributed to the intricate $BrONO_2$ hydrolysis mechanism, which extends beyond the small fluctuations in the $O_3/(HO_2+RO_2)$ ratio in the relatively colder climate of a glacial period (Geng et al., 2017). Thus, reactive halogen chemistry may also be a factor that impacts changes in the atmospheric oxidizing capacity, specifically in high-latitude regions in the Northern Hemisphere.

4.4 Comparisons with other ice core data

The $\delta^{15}N(NO_3^-)$ value of ice cores collected in Lomonosovfonna, Svalbard, was –6.9 ± 1.9 ‰ after 1950 (Vega et al., 2015), which is lower than that at the SE-Dome and Summit. Given that snow accumulation at Lomonosovfonna (0.55 ± 0.1 m w e a^{-1}, Vega et al., 2015) was higher than at the Summit, these low $\delta^{15}N(NO_3^-)$ values may reflect less post-depositional alterations. Notably, the relatively low $\delta^{15}N(NO_3^-)$ values at Lomonosovfonna and the SE-Dome were consistent with the low $\delta^{15}N(NO_3^-)$ values in aerosols observed at two Arctic stations (Morin et al., 2008, 2012). Notably, the SE-Dome and Svalbard both had lower $\delta^{15}N(NO_3^-)$ values and higher accumulation rates than the Summit. Additionally, Svalbard is closer to Europe than Greenland, which may indicate a regional source difference. Ice-core $\delta^{15}N(NO_3^-)$ records reported from the Lomonosovfonna also exhibited decreasing trends until the 1970s, whereas an increase in $\delta^{15}N(NO_3^-)$ was only observed at Lomonosovfonna after the 1990s (Vega et al., 2015). Such differences may be attributed to differences in NO_x sources and spatial chemistries in the Arctic, although it is unclear whether this difference was caused by anthropogenic sources, natural sources, transport, or a combination of these factors.

$\delta^{15}N(NO_3^-)$ records in ice cores from the Tibetan Plateau also exhibit decreasing trends from 1955 to 2011 (Li et al., 2020). The $\delta^{15}N(NO_3^-)$ of this Tibetan Plateau ice core (4.2 ± 3.1 ‰ in 1951–2011) is also substantially higher than those of Arctic ice cores, indicating a different regional context. Comparing $\delta^{15}N(NO_3^-)$ records from different locations would be beneficial for determining the regional physical/chemical behaviors of NO_3^- from emission to deposition. This would allow us to better assess the impacts of human activity on nitrogen cycling and take corresponding measures to reduce the adverse effects of NO_3^- on climate and biogeochemical cycles. However, in Antarctica (Akers et al., 2022), the ice-core $\delta^{15}N(NO_3^-)$ values varied significantly depending on the snow accumulation rate. It is therefore important to estimate post-depositional alteration for each ice core, refine models with recent information (Shi et al., 2023), and perform reverse calculations for atmospheric $\delta^{15}N(NO_3^-)$ (Jiang et al., 2024). The TRANSITS model used in this study is effective for assessing the sensitivity of nitrate preservation and isotopic compositions to snow accumulation within the same environment. However, as discussed, the archived isotopic composition depends on the f_{exp} value, which varies spatiotemporally. Therefore, efforts should be made to update models that account for photolysis of snow $NO_3^-$and the recycling and redistribution of reactive nitrogen in boundary layer chemistry within global chemical transport model (Zatko et al., 2016) by incorporating $\delta^{15}N$ information. Additionally, a recent study emphasized the potential impact of microbial alterations to both NO_3^- concentrations and its isotopic compositions in an Asian glacier (Hattori et al., 2023); thus, interpretations of NO_3^- concentrations and $\delta^{15}N(NO_3^-)$ records in ice cores should proceed with caution. We recommend that interpretations of NO_3^- concentrations and $\delta^{15}N(NO_3^-)$ records in ice cores should be accompanied by $\Delta^{17}O(NO_3^-)$ or $\delta^{18}O(NO_3^-)$ records whenever possible to verify atmospheric NO_3^- preservation without post-depositional biological alteration.

5 Conclusions

In this study, we reported ~60-year (1959–2014) records of NO_3^- isotopic compositions from the SE-Dome ice core in Greenland. The observed $\delta^{15}N(NO_3^-)$ values in the SE-Dome ice core were consistently ~4 ‰ lower than those in the Summit ice core record. The high snow accumulation rate at the SE-Dome site reduces the sensitivity of NO_3^- to post-depositional processes, which was supported by outputs from the TRANSITS model. Therefore, we concluded that the SE-Dome ice core, which exhibits superior NO_3^- preservation, is a promising tool for reconstructing changes in atmospheric nitrogen cycling driven by anthropogenic activity. This study was based on results from the SE-Dome I ice core (~90 m), which covers the past 60 years. The SE-Dome II core (drilled in 2021) preserves records that extend back to 1800 CE (Iizuka et al., 2021; Kawakami et al., 2023). Thus, there is considerable potential for future research aimed at reconstructing NO_3^- aerosol dynamics from the beginning of the Industrial Revolution to the present. Additionally, while regional comparisons of ice-core $\delta^{15}N(NO_3^-)$ records are beneficial for describing the regional physicochemical behaviours of NO_3^-, it is necessary to account for regional differences in post-depositional alteration when analysing the spatiotemporal variations in atmospheric NO_3^- isotopes.

Data availability

The data used in this study named "Figure_data_file_final" will be available in the Hokkaido University Collection of Scholarly and Academic Papers (https://eprints.lib.hokudai.ac.jp/dspace/) once the paper is accepted.

Author contributions

SH conceptualized the study; ZW, SH, AT, SI, ZJ, SM, and YI curated the data; ZW, SH, AT, ZJ, SI, and YI performed the formal analysis; SH and YI acquired funding; SH, AT, NY, KF, SI, SM, and YI conducted the investigation; SH, ZJ, LG, and JS developed the methodology; SH managed the project; ZW and SH validated the results; ZW, KF, SH, and ZJ visualized the data; ZW and SH wrote the original draft; KF, SI, ZJ, LG, JS, RU, AL, and YI reviewed and edited the manuscript.

Competing interests

The authors declare no conflicts of interest.

Acknowledgements

The authors gratefully acknowledge the NOAA Air Resources Laboratory (ARL) for providing the HYSPLIT transport and dispersion model (Stein et al., 2015). We acknowledge Jihong Cole-Dai for providing data on the annual snow accumulation rate at the Summit.

Financial support

This study was supported by the National Natural Science Foundation of China (Grant Nos. W2441015, 42494851, and 42473011), the Fundamental Research Funds for the Central Universities, including the General Program (Grant No. 0206/14380918), the International Collaboration Program (Grant No. 0206/14380225), the Cemac "GeoX" Interdisciplinary Program (Grant No. 0206/14380205), and additional grants (Nos. 0206/143802024, 0206/14380150, 0206/14380185, and 0206/14380174), as well as start-up funding from Nanjing University. This study was also supported by MEXT/JSPS KAKENHI [Grant nos. 18H05292, 23H00511, and 23K18516] and the Arctic Challenge for Sustainability (ArCS II) Project [Program Grant no. JPMXD1420318865]. This study was performed under the cooperative research program of the Institute of Nature and Environmental Technology, Kanazawa University [Project no. 22042, 23039]. S.H. was supported by MEXT/JSPS KAKENHI [Grant no. 20H04305].

Table 1. Parameters used in the Transfer of Atmospheric Nitrate Stable Isotopes To the Snow (TRANSITS) model for the SE-Dome ice core

Parameters	Description	Value	Unit	Data origin
ρ	Snow density	400	kg m^{-3}	Oyabu et al., (2016)
SSA	Snow-specific surface area	47.0	m^2 kg^{-1}	Domine et al., (2007)
$[BC]_{SE\text{-}Dome}$	BC concentration	2.2	ng g^{-1}	See text
[Dust]	Dust concentration	33.94	ng g^{-1}	Amino et al., (2021)
$[HULIS]_{SE\text{-}Dome}$	HULIS concentration	47.6	ng g^{-1}	See text
TCO	Total column ozone	See Supplement data file 1	DU	Jiang et al., (2021)
h	Boundary layer height	See Supplement data file 1	m	ERA5(Hersbach et al., (2020); Khalzan et al., (2022)
T	Temperature		°C	
P	Pressure		hPa	
$[O_3]$	O_3 concentration	26.66 ~ 32.30	ppb	GEOS-Chem v12.9.3 (https://doi.org/10.5281/zenodo.3974569, last access 30 August 2023)
[BrO]	BrO concentration	0.06 ~ 0.76	ppt	
$[OH]/[HO_2]$	OH/HO_2 concentration	See Supplement data file 1	ppt	
A	Snow accumulation	101	cm a^{-1}	Iizuka et al., (2017)
F_{pri}	Primary Nitrate flux	16.28	kg N m^{-2} a^{-1}	Iizuka et al., (2018)
f_{exp}	Export fraction	47%	–	See Table S2.
$^{15}\varepsilon_p$	N isotope fractionation constant during photolysis	$^{15}\varepsilon_p=J^{15}/J^{14}$-1	‰	Erbland et al., (2013)
$^{15}\varepsilon_d$	N isotope fractionation constant during deposition	10	‰	
f_{cage}	Cage effect	15	%	Erbland et al., (2015)

References

Akers, P. D., Savarino, J., Caillon, N., Servettaz, A. P. M., Le Meur, E., Magand, O., Martins, J., Agosta, C., Crockford, P., Kobayashi, K., Hattori, S., Curran, M., van Ommen, T., Jong, L., and Roberts, J. L.: Sunlight-driven nitrate loss records Antarctic surface mass balance, *Nat. Commun.*, 13, 4274, doi:10.1038/s41467-022-31855-7, 2022.

Alexander, B., Savarino, J., Kreutz, K. J., and Thiemens, M. H.: Impact of preindustrial biomass-burning emissions on the oxidation pathways of tropospheric sulfur and nitrogen, *J. Geophys. Res. Atmos.*, 109, doi:10.1029/2003JD004218, 2004.

Alexander, B., Hastings, M. G., Allman, D. J., Dachs, J., Thornton, J. A., and Kunasek, S. A.: Quantifying atmospheric nitrate formation pathways based on a global model of the oxygen isotopic composition ($\Delta^{17}O$) of atmospheric nitrate, *Atmos. Chem. Phys.*, 9, 5043–5056, doi:10.5194/acp-9-5043-2009, 2009.

Alexander, B., Sherwen, T., Holmes, C. D., Fisher, J. A., Chen, Q., Evans, M. J., and Kasibhatla, P.: Global inorganic nitrate production mechanisms: comparison of a global model with nitrate isotope observations, *Atmos. Chem. Phys.*, 20, 3859–3877, doi:10.5194/acp-20-3859-2020, 2020.

Amino, T., Iizuka, Y., Matoba, S., Shimada, R., Oshima, N., Suzuki, T., Ando, T., Aoki, T., and Fujita, K.: Increasing dust emission from ice free terrain in southeastern Greenland since 2000, *Polar Sci.*, 27, 100599, doi:10.1016/j.polar.2020.100599, 2021.

Bekker, C., Walters, W. W., Murray, L. T., and Hastings, M. G.: Nitrate chemistry in the northeast US – Part 1: Nitrogen isotope seasonality tracks nitrate formation chemistry, *Atmos. Chem. Phys.*, 23, 4185-4201, doi:10.5194/acp-23-4185-2023, 2023.

Burkhart, J. F., Hutterli, M., Bales, R. C., and McConnell, J. R.: Seasonal accumulation timing and preservation of nitrate in firn at Summit, Greenland, *J. Geophys. Res. Atmos.*, 109, doi:10.1029/2004JD004658, 2004.

Berhanu, T. A., Meusinger, C., Erbland, J., Jost, R., Bhattacharya, S. K., Johnson, M. S., and Savarino, J.: Laboratory study of nitrate photolysis in Antarctic snow. II. Isotopic effects and wavelength dependence, *J. Chem. Phys.*, 140, 244306, doi:10.1063/1.4882899, 2014.

Berhanu, T. A., Savarino, J., Erbland, J., Vicars, W. C., Preunkert, S., Martins, J. F., and Johnson, M. S.: Isotopic effects of nitrate photochemistry in snow: a field study at Dome C, Antarctica, *Atmos. Chem. Phys.*, 15, 11243–11256, doi:10.5194/acp-15-11243-2015, 2015.

Beyn, F., Matthias, V., and Dähnke, K.: Changes in atmospheric nitrate deposition in Germany – An isotopic perspective, *Environ. Pollut.*, 194, 1–10, doi:10.1016/j.envpol.2014.06.043, 2014.

Chai, J., Miller, D. J., Scheuer, E., Dibb, J., Selimovic, V., Yokelson, R., Zarzana, K. J., Brown, S. S., Koss, A. R., Warneke, C., and Hastings, M.: Isotopic characterization of nitrogen oxides (NO_x), nitrous acid (HONO), and nitrate (pNO_3^-) from laboratory biomass burning during FIREX, *Atmos. Meas. Tech.*, 12, 6303–6317, https://doi.org/10.5194/amt-12-6303-2019, 2019.

Dibb, J. E., and Fahnestock, M.: Snow accumulation, surface height change, and firn densification at Summit, Greenland: Insights from 2 years of in situ observation, *J. Geophys. Res. Atmos.*, 109, D24113, doi:10.1029/2003JD004300, 2004.

Domine, F., Taillandier, A. S., and Simpson, W. R.: A parameterization of the specific surface area of seasonal snow for field use and for models of snowpack evolution, *J. Geophys. Res. Earth Surf.*, 112, doi:10.1029/2006JF000512, 2007.

Duce, R. A., LaRoche, J., Altieri, K., Arrigo, K. R., Baker, A. R., Capone, D. G., Cornell, S., Dentener, F., Galloway, J., Ganeshram, R. S., Geider, R. J., Jickells, T., Kuypers, M. M., Langlois, R., Liss, P. S., Liu, S. M., Middelburg, J. J., Moore, C. M., Nickovic, S., Oschlies, A., Pedersen, T., Prospero, J., Schlitzer, R., Seitzinger, S., Sorensen, L. L., Uematsu, M., Ulloa, O., Voss, M., Ward, B., and Zamora, L.: Impacts of atmospheric anthropogenic nitrogen on the open ocean, *Science*, 320, 893–897, doi:10.1126/science.1150369, 2008.

Eichler, A., Legrand, M., Jenk, T. M., Preunkert, S., Andersson, C., Eckhardt, S., Engardt, M., Plach, A., and Schwikowski, M.: Consistent histories of anthropogenic western European air pollution preserved in different Alpine ice cores, *Cryosphere*, 17(5), 2119–2137, doi: 10.5194/tc-17-2119-2023, 2023.

Elliott, E. M., Yu, Z., Cole, A. S., and Coughlin, J. G.: Isotopic advances in understanding reactive nitrogen deposition and atmospheric processing, *Sci. Total Environ.*, 662, 393–403, doi:https://doi.org/10.1016/j.scitotenv.2018.12.177, 2019.

Erbland, J., Vicars, W. C., Savarino, J., Morin, S., Frey, M. M., Frosini, D., Vince, E., and Martins, J. M. F.: Air–snow transfer of nitrate on the East Antarctic Plateau – Part 1: Isotopic evidence for a photolytically driven dynamic equilibrium in summer, *Atmos. Chem. Phys.*, 13, 6403–6419, doi:10.5194/acp-13-6403-2013, 2013.

Erbland, J., Savarino, J., Morin, S., France, J. L., Frey, M. M., and King, M. D.: Air–snow transfer of nitrate on the East Antarctic Plateau – Part 2: An isotopic model for the interpretation of deep ice-core records, *Atmos. Chem. Phys.*, 15, 12079-12113, doi:10.5194/acp-15-12079-2015, 2015.

Felix, J. D., and Elliott, E. M.: The agricultural history of human-nitrogen interactions as recorded in ice core δ^{15}N-NO_3^-, *Geophys. Res. Lett.*, 40, 1642-1646, doi:10.1002/grl.50209, 2013.

Freyer, H. D.: Seasonal variation of 15N/14N ratios in atmospheric nitrate species, *Tellus B*, 43, 30-44, doi:10.1034/j.1600-0889.1991.00003.x, 1991.

Freyer, H. D., Kobel, K., Delmas, R. J., Kley, D., and Legrand, M. R.: First results of ^{15}N/^{14}N ratios in nitrate from alpine and polar ice cores, *Tellus B*, 48, 93-105, doi:10.1034/j.1600-0889.1996.00009.x, 1996.

Fibiger, D. L., Dibb, J. E., Chen, D., Thomas, J. L., Burkhart, J. F., Huey, L. G., and Hastings, M. G.: Analysis of nitrate in the snow and atmosphere at Summit, Greenland: Chemistry and transport, *J. Geophys. Res. Atmos.*, 121, 5010-5030, doi:10.1002/2015JD024187, 2016.

Finlayson-Pitts, B. J., and Pitts, J. N.: Chemistry of the upper and lower atmosphere: Theory, experiments, and applications, San Diego: Academic Press, 2000.

Frey, M. M., Savarino, J., Morin, S., Erbland, J., and Martins, J.: Photolysis imprint in the nitrate stable isotope signal in snow and atmosphere of East Antarctica and implications for reactive nitrogen cycling, *Atmos. Chem. Phys.*, 9, 8681-8696, doi:10.5194/acp-9-8681-2009, 2009.

Furukawa, R., Uemura, R., Fujita, K., Sjolte, J., Yoshimura, K., Matoba, S., and Iizuka, Y.: Seasonal-scale dating of a shallow ice core from Greenland using oxygen isotope matching between data and simulation, *J. Geophys. Res. Atmos.*, 122, 873-887, doi:10.1002/2017jd026716, 2017.

Geng, L., Alexander, B., Cole-Dai, J., Steig, E. J., Savarino, J., Sofen, E. D., and Schauer, A. J.: Nitrogen isotopes in ice core nitrate linked to anthropogenic atmospheric acidity change, *Proc. Natl. Acad. Sci. USA*, 111, 5808-5812, doi:10.1073/pnas.1319441111, 2014.

Geng, L., Zatko, M. C., Alexander, B., Fudge, T. J., Schauer, A. J., Murray, L. T., and Mickley, L. J.: Effects of post-depositional processing on nitrogen isotopes of nitrate in the Greenland Ice Sheet Project 2 ice core, *Geophys. Res. Lett.*, 5346-5354, doi:10.1002/2015gl064218, 2015.

Hastings, M. G., Sigman, D. M., and Steig, E. J.: Glacial/interglacial changes in the isotopes of nitrate from the Greenland Ice Sheet Project 2 (GISP2) ice core, *Global Biogeochem. Cycles*, 19, GB4024, doi:10.1029/2005GB002502, 2005.

Hastings, M. G., Jarvis, J. C., and Steig, E. J.: Anthropogenic impacts on nitrogen isotopes of ice-core nitrate, *Science*, 324, 1288, doi:10.1126/science.1170510, 2009.

Hastings, M. G.: Evaluating source, chemistry and climate change based upon the isotopic composition of nitrate in ice cores, *IOP Conf. Ser.: Earth Environ. Sci.*, 9, 012002, doi:10.1088/1755-1315/9/1/012002, 2010.

Hastings, M. G., Casciotti, K. L., and Elliott, E. M.: Stable isotopes as tracers of anthropogenic nitrogen sources, deposition, and impacts, *Elements*, 339–344, doi:10.2113/gselements.9.5.339, 2013.

Hattori, S., Savarino, J., Kamezaki, K., Ishino, S., Dyckmans, J., Fujinawa, T., Caillon, N., Barbero, A., Mukotaka, A., Toyoda, S., Well, R., and Yoshida, N.: Automated system measuring triple oxygen and nitrogen isotope ratios in nitrate using the bacterial method and N2O decomposition by microwave discharge, *Rapid Commun. Mass Spectrom.*, 30, 2635-2644, doi:10.1002/rcm.7747, 2016.

Hattori, S., Iizuka, Y., Alexander, B., Ishino, S., Fujita, K., Zhai, S., Sherwen, T., Oshima, N., Uemura, R., Yamada, A., Suzuki, N., Matoba, S., Tsuruta, A., Savarino, J., and Yoshida, N.: Isotopic evidence for acidity-driven enhancement of sulfate formation after SO2 emission control, *Sci. Adv.*, 7, eabd4610, doi:10.1126/sciadv.abd4610, 2021.

Hattori, S., Li, Z. Q., Yoshida, N., and Takeuchi, N.: Isotopic evidence for microbial nitrogen cycling in a glacier interior of high-mountain Asia, *Environ. Sci. Technol.*, 57, 15026-15036, doi:10.1021/acs.est.3c04757, 2023.

Heaton, T. H. E.: Ratios of nitrate and ammonium in rain at Pretoria, South Africa, *Atmos. Environ.*, 21, 843-852, doi:10.1016/0004-6981(87)90080-1, 1987.

Hersbach, H., Bell, B., Berrisford, P., Hirahara, S., Horányi, A., Muñoz-Sabater, J., Nicolas, J., Peubey, C., Radu, R., Schepers, D., Simmons, A., Soci, C., Abdalla, S., Abellan, X., Balsamo, G., Bechtold, P., Biavati, G., Bidlot, J., Bonavita, M., De Chiara, G., Dahlgren, P., Dee, D., Diamantakis, M., Dragani, R., Flemming, J., Forbes, R., Fuentes, M., Geer, A., Haimberger, L., Healy, S., Hogan, R. J., Holm, E., Janisková, M., Keeley, S., Laloyaux, P., Lopez, P., Lupu, C., Radnoti, G., de Rosnay, P., Rozum, I., Vamborg, F., Villaume, S., and Thépaut, J.-N.: The ERA5 global reanalysis, *Q. J. R. Meteorol. Soc.*, 146, 1999-2049, doi:10.1002/qj.3803, 2020.

Iizuka, Y., Miyamoto, A., Hori, A., Matoba, S., Furukawa, R., Saito, T., Fujita, S., Hirabayashi, M., Yamaguchi, S., Fujita, K., and Takeuchi, N.: A firn densification process in the high accumulation dome of Southeastern Greenland, *Arct. Antarct. Alp. Res.*, 49, 13-27, doi:10.1657/AAAR0016-034, 2017.

Iizuka, Y., Uemura, R., Fujita, K., Hattori, S., Seki, O., Miyamoto, C., Suzuki, T., Yoshida, N., Motoyama, H., and Matoba, S.: A 60 year record of atmospheric aerosol depositions preserved in a high-accumulation dome ice core, Southeast Greenland, *J. Geophys. Res. Atmos.*, 123, 574-589, doi:10.1002/2017JD026733, 2018.

Iizuka, Y., Matoba, S., Minowa, M., Yamasaki, T., Kawakami, K., Kakugo, A., Miyahara, M., Hashimoto, A., Niwano, M., Tanikawa, T., Fujita, K., and Aoki, T.: Ice core drilling and the related observations at SE-Dome site, Southeastern Greenland Ice Sheet, *Bull. Glaciol. Res.*, 39, 1-12, doi:10.5331/bgr.21R01, 2021.

Jarvis, J. C., Hastings, M. G., Steig, E. J., and Kunasek, S. A.: Isotopic ratios in gas-phase HNO3 and snow nitrate at Summit, Greenland, *J. Geophys. Res. Atmos.*, 114, D17301, doi:10.1029/2009JD012134, 2009.

Jiang, Z., Alexander, B., Savarino, J., Erbland, J., and Geng, L.: Impacts of the photo-driven post-depositional processing on snow nitrate and its isotopes at Summit, Greenland: a model-based study, *Cryosphere*, 15, 4207-4220, doi:10.5194/tc-15-4207-2021, 2021.

Jiang, Z., Alexander, B., Savarino, J., and Geng, L.: An inverse model to correct for the effects of post-depositional processing on ice-core nitrate and its isotopes: Model framework and applications at Summit, Greenland and Dome C, Antarctica, *Atmos. Chem. Phys.*, 24, 4895-4914, doi:10.5194/acp-24-4895-2024, 2024.

Kahl, J. D. W., Martinez, D. A., Kuhns, H., Davidson, C. I., Jaffrezo, J.-L., and Harris, J. M.: Air mass trajectories to Summit, Greenland: A 44-year climatology and some episodic events, *J. Geophys. Res. Oceans*, 102, 26861-26875, doi:10.1029/97JC00296, 1997.

Kawakami, K., Iizuka, Y., Sasage, M., Matsumoto, M., Saito, T., Hori, A., and Matoba, S.: SE-Dome II ice core dating with half-year precision: increasing melting events from 1799 to 2020 in Southeastern Greenland, *J. Geophys. Res. Atmos.*, 128, e2023JD038874, doi:10.1029/2023JD038874, 2023.

Kendall, M. G.: Rank correlation measures, Charles Griffin, 1975.

Khalzan, P., Sakai, A., and Fujita, K.: Mass balance of four mongolian glaciers: in-situ measurements, long-term reconstruction and sensitivity analysis, *Front. Earth Sci.*, 9, 785306, doi:10.3389/feart.2021.785306, 2022.

Law, K., Hjorth, J., Pernov, J., Whaley, C., Skov, H., Coen, M., and Zhang, K.: Arctic tropospheric ozone trends, *Geophys. Res. Lett.*, 50, e2023GL103096, doi:10.1029/2023GL103096, 2023.

Li, Z., Hastings, M. G., Walters, W. W., Tian, L., Clemens, S. C., Song, L., and Fang, Y.: Isotopic evidence that recent agriculture overprints climate variability in nitrogen deposition to the Tibetan Plateau, *Environ. Int.*, 138, 105614, doi:10.1016/j.envint.2020.105614, 2020.

Lim, S., Lee, M., Savarino, J., and Laj, P.: Oxidation pathways and emission sources of atmospheric particulate nitrate in Seoul: based on δ^{15}N and Δ^{17}O measurements, *Atmos. Chem. Phys.*, 22, 5099-5115, doi:10.5194/acp-22-5099-2022, 2022.

Mann, H. B.: Non-parametric tests against trend, *Econometrica*, 13, 245-259, doi:10.2307/1907187, 1945.

Mayewski, P. A., Lyons, W. B., Spencer, M. J., Twickler, M., Dansgaard, W., Koci, B., and Honrath, R. E.: Sulfate and nitrate concentrations from a south Greenland ice core, *Science*, 232, 975-977, doi:10.1126/science.232.4753.975, 1986.

McCabe, J. R., Boxe, C. S., Colussi, A. J., Hoffmann, M. R., and Thiemens, M. H.: Oxygen isotopic fractionation in the photochemistry of nitrate in water and ice, *J. Geophys. Res. Atmos.*, 110, 148-227, doi:10.1029/2004JD005484, 2005.

McIlvin, M. R., and Casciotti, K. L.: Technical updates to the bacterial method for nitrate isotopic analyses, *Anal. Chem.*, 83(5), 1850–1856, doi: 10.1021/ac1028984, 2011.

Meusinger, C., Berhanu, T. A., Erbland, J., Savarino, J., and Johnson, M. S.: Laboratory study of nitrate photolysis in Antarctic snow. I. Observed quantum yield, domain of photolysis, and secondary chemistry, *J. Chem. Phys.*, 140, 244305, doi:10.1063/1.4882898, 2014.

Michalski, G., Scott, Z., Kabiling, M., and Thiemens, M. H.: First measurements and modeling of Δ^{17}O in atmospheric nitrate, *Geophys. Res. Lett.*, 30, 1870, doi:10.1029/2003GL017015, 2003.

Michalski, G., Bhattacharya, S. K., and Mase, D. F.: Oxygen Isotope Dynamics of Atmospheric Nitrate and Its Precursor Molecules, in: Handbook of Environmental Isotope Geochemistry, edited by: Baskaran, M., Advances in Isotope Geochemistry, Springer, Berlin, Heidelberg, doi:10.1007/978-3-642-10637-8_30, 2012.

Morin, S., Savarino, J., Frey, M. M., Yan, N., Bekki, S., Bottenheim, J. W., and Martins, J. M.: Tracing the origin and fate of NOx in the Arctic atmosphere using stable isotopes in nitrate, *Science*, 322, 730-732, doi:10.1126/science.1161910, 2008.

Morin, S., Savarino, J., Frey, M. M., Domine, F., Jacobi, H. W., Kaleschke, L., and Martins, J. M. F.: Comprehensive isotopic composition of atmospheric nitrate in the Atlantic Ocean boundary layer from 65°S to 79°N, *J. Geophys. Res. Atmos.*, 114, D05303, doi:10.1029/2008JD010696, 2009.

Morin, S., Erbland, J., Savarino, J., Domine, F., Bock, J., Friess, U., Jacobi, H.-W., Sihler, H., and Martins, J. M. F.: An isotopic view on the connection between photolytic emissions of NOx from the Arctic snowpack and its oxidation by reactive halogens, *J. Geophys. Res. Atmos.*, 117, D00R08, doi:10.1029/2011JD016618, 2012.

Neftel, A., Moor, E., Oeschger, H., and Stauffer, B.: Evidence from polar ice cores for the increase in atmospheric CO_2 in the past two centuries, *Nature*, 315, 45-47, doi:10.1038/315045a0, 1985.

Noro, K., Hattori, S., Uemura, R., Fukui, K., Hirabayashi, M., Kawamura, K., Motoyama, H., Takenaka, N., and Yoshida, N.: Spatial variation of isotopic compositions of snowpack nitrate related to post-depositional processes in eastern Dronning Maud Land, East Antarctica, *Geochem. J.*, 52, e7-e14, doi:10.2343/geochemj.2.0519, 2018.

Oyabu, I., Matoba, S., Yamasaki, T., Kadota, M., and Iizuka, Y.: Seasonal variations in the major chemical species of snow at the Southeast Dome in Greenland, *Polar Sci.*, 10, 36-42, doi:10.1016/j.polar.2016.01.003, 2016.

Parvin, F., Seki, O., Fujita, K., Iizuka, Y., Matoba, S., Ando, T., and Sawada, K.: Assessment for paleoclimatic utility of biomass burning tracers in SE-Dome ice core, Greenland, *Atmos. Environ.*, 196, 86-94, doi:10.1016/j.atmosenv.2018.10.012, 2019.

Röthlisberger, R., Hutterli, M. A., Sommer, S., Wolff, E. W., and Mulvaney, R.: Factors controlling nitrate in ice cores: Evidence from the Dome C deep ice core, *J. Geophys. Res. Atmos.*, 105, 20565-20572, doi:10.1029/2000JD900264, 2000.

Röthlisberger, R., Hutterli, M. A., Wolff, E. W., Mulvaney, R., Fischer, H., Bigler, M., Goto-Azuma, K., Hansson, M. E., Ruth, U., Siggaard-Andersen, M.-L., and Steffensen, J. P.: Nitrate in Greenland and Antarctic ice cores: a detailed description of post-depositional processes, *Ann. Glaciol.*, 35, 209-216, doi:10.3189/172756402781817220, 2002.

Savarino, J., Kaiser, J., Morin, S., Sigman, D. M., and Thiemens, M. H.: Nitrogen and oxygen isotopic constraints on the origin of atmospheric nitrate in coastal Antarctica, *Atmos. Chem. Phys.*, 7, 1925-1945, doi:10.5194/acp-7-1925-2007, 2007.

Sigman, D. M., Casciotti, K. L., Andreani, M., Barford, C., Galanter, M., and Böhlke, J. K.: A Bacterial Method for the Nitrogen Isotopic Analysis of Nitrate in Seawater and Freshwater, *Anal. Chem.*, 73(17), 4145–4153, doi: 10.1021/ac010088e, 2001

Shammas, N. K., Wang, L. K., and Wang, M. H. S.: Sources, chemistry and control of acid rain in the environment, in: Handbook of Environment and Waste Management, 1-26, doi:10.1142/9789811207136_0001, 2020.

Shi, G., Ma, H., Zhu, Z., Hu, Z., Chen, Z., Jiang, S., An, C., Yu, J., Ma, T., Li, Y., Sun, B., and Hastings, M. G.: Using stable isotopes to distinguish atmospheric nitrate production and its contribution to the surface ocean across hemispheres, *Earth Planet. Sci. Lett.*, 564, 116914, doi:10.1016/j.epsl.2021.116914, 2021.

Shi, G., Buffen, A. M., Hu, Y., Chai, J., Li, Y., Wang, D., and Hastings, M. G.: Modeling the complete nitrogen and oxygen isotopic imprint of nitrate photolysis in snow, *Geophys. Res. Lett.*, 50, e2023GL103778, doi:10.1029/2023GL103778, 2023.

Song, W., Liu, X. Y., Hu, C. C., Chen, G. Y., Liu, X. J., Walters, W. W., Michalski, G., and Liu, C. Q.: Important contributions of non-fossil fuel nitrogen oxides emissions, *Nat. Commun.*, 12, 243, doi:10.1038/s41467-020-20356-0, 2021.

Stein, A. F., Draxler, R. R., Rolph, G. D., Stunder, B. J. B., Cohen, M. D., and Ngan, F.: NOAA's HYSPLIT atmospheric transport and dispersion modeling system, *Bull. Am. Meteorol. Soc.*, 96, 2059-2077, doi:10.1175/BAMS-D-14-00110.1, 2015.

Vega, C. P., Pohjola, V. A., Samyn, D., Pettersson, R., Isaksson, E., Björkman, M. P., Martma, T., Marca, A., and Kaiser, J.: First ice core records of NO_3^- stable isotopes from Lomonosovfonna, Svalbard, *J. Geophys. Res. Atmos.*, 120, 313-330, doi:10.1002/2013JD020930, 2015.

Vicars, W., and Savarino, J.: Quantitative constraints on the 17O-excess (Δ17O) signature of surface ozone: Ambient measurements from 50°N to 50°S using the nitrite-coated filter technique, *Geochim. Cosmochim. Acta*, 135, 270-287, doi:10.1016/j.gca.2014.03.023, 2014.

Walters, W. W., and Michalski, G.: Theoretical calculation of nitrogen isotope equilibrium exchange fractionation factors for various NOy molecules, *Geochim. Cosmochim. Acta*, 164, 284-297, doi:10.1016/j.gca.2015.05.029, 2015a.

Walters, W. W., Goodwin, S. R., and Michalski, G.: Nitrogen stable isotope composition ($\delta^{15}N$) of vehicle-emitted NOx, *Environ. Sci. Technol.*, 49, 2278-2285, doi:10.1021/es505580v, 2015b.

Walters, W. W., and Michalski, G.: Theoretical calculation of oxygen equilibrium isotope fractionation factors involving various NOy molecules, OH, and H2O and its implications for isotope variations in atmospheric nitrate, *Geochim. Cosmochim. Acta*, 191, 89-101, doi:10.1016/j.gca.2016.06.039, 2016.

Zatko, M., Geng, L., Alexander, B., Sofen, E., and Klein, K.: The impact of snow nitrate photolysis on boundary layer chemistry and the recycling and redistribution of reactive nitrogen across Antarctica and Greenland in a global chemical transport model, *Atmos. Chem. Phys.*, 16, 2819-2842, doi:10.5194/acp-16-2819-2016, 2016.

Zhai, S., Jacob, D. J., Wang, X., Liu, Z., Wen, T., Shah, V., Li, K., Moch, J. M., Bates, K. H., Song, S., Shen, L., Zhang, Y., Luo, G., Yu, F., Sun, Y., Wang, L., Qi, M., Tao, J., Gui, K., Xu, H., Zhang, Q., Zhao, T., Wang, Y., Lee, H. C., Choi, H., and Liao, H.: Control of particulate nitrate air pollution in China, *Nat. Geosci.*, 14, 389-395, doi:10.1038/s41561-021-00726-z, 2021.